energy of the chlorine ion at 500 pA, compared with the 100 pA case, results in the more extended radial distribution and, because of surface scattering, the more isotropic angular distribution of the chlorine daughters. □

Received 7 December 2004; accepted 20 January 2005; doi:10.1038/nature03385.

1. Eigler, D. M. & Schweizer, E. K. Positioning single atoms with a scanning tunnelling microscope. *Nature* **344,** 524–526 (1990).
2. Bartels, L., Meyer, G. & Rieder, K.-H. Basic steps of lateral manipulation of single atoms and diatomic clusters with a scanning tunneling microscope tip. *Phys. Rev. Lett.* **79,** 697–700 (1997).
3. Komeda, T., Kim, Y., Kawai, M., Persson, B. N. J. & Ueba, H. Lateral hopping of molecules induced by excitation of internal vibration mode. *Science* **295,** 2055–2058 (2002).
4. Pascual, J. I., Lorente, N., Song, Z., Conrad, H. & Rust, H.-P. Selectivity in vibrationally mediated single-molecule chemistry. *Nature* **423,** 525–528 (2003).
5. Fishlock, T. W., Oral, A., Egdell, R. G. & Pethica, J. B. Manipulation of atoms across a surface at room temperature. *Nature* **404,** 743–745 (2000).
6. Salam, G. P., Persson, M. & Palmer, R. E. Possibility of coherent multiple excitation in atom transfer with a scanning tunneling microscope. *Phys. Rev. B* **49,** 10655–10662 (1994).
7. Stipe, B. C. *et al.* Single-molecule dissociation by tunneling electrons. *Phys. Rev. Lett.* **78,** 4410–4413 (1997).
8. Lauhon, L. J. & Ho, W. Control and characterization of a multistep unimolecular reaction. *Phys. Rev. Lett.* **84,** 1527–1530 (2000).
9. Hla, S.-W., Bartels, L., Meyer, G. & Rieder, K.-H. Inducing all steps of a chemical reaction with the scanning tunneling microscope tip: Towards single molecule engineering. *Phys. Rev. Lett.* **85,** 2777–2780 (2000).
10. Lu, P. H., Polanyi, J. C. & Rogers, D. Electron-induced "localized atomic reaction" (LAR): chlorobenzene adsorbed on Si(111) 7 × 7. *J. Chem. Phys.* **111,** 9905–9907 (1999).
11. Soukiassian, L., Mayne, A. J., Carbone, M. & Dujardin, G. Atomic-scale desorption of H atoms from the Si(100)-2 × 1:H surface: inelastic electron interactions. *Phys. Rev. B* **68,** 035303 (2003).
12. Boland, J. J. & Villarrubia, J. S. Formation of Si(111)-(1 × 1)Cl. *Phys. Rev. B* **41,** 9865–9870 (1990).
13. Nakamura, Y., Mera, Y. & Maeda, K. Diffusion of chlorine atoms on Si(111)-(7 × 7) surface enhanced by electron injection from scanning tunneling microscope tips. *Surf. Sci.* **487,** 127–134 (2001).
14. Brune, H., Wintterlin, J., Behm, R. J. & Ertl, G. Surface migration of "hot" adatoms in the course of dissociative chemisorption of oxygen on Al(111). *Phys. Rev. Lett.* **68,** 624–626 (1992).
15. Cao, Y., Deng, J. F. & Xu, G. Q. Stereo-selective binding of chlorobenzene on Si(111)-7 × 7. *J. Chem. Phys.* **112,** 4759–4767 (2000).
16. Sloan, P. A., Hedouin, M. F. G., Palmer, R. E. & Persson, M. Mechanism of molecular manipulation with the scanning tunneling microscope at room temperature: chlorobenzene/Si(111)-(7 × 7). *Phys. Rev. Lett.* **91,** 118301 (2003).
17. Li, Z.-H., Li, Y.-C., Wang, W.-N., Cao, Y. & Fan, K.-N. A density functional theory study on the adsorption of chlorobenzene on the Si(111)-7 × 7 surface. *J. Phys. Chem. B* **108,** 14049–14055 (2004).
18. Jensen, J. A., Yan, C. & Kummel, A. C. Direct chemisorption site selectivity for molecular halogens on the Si(111)-(7 × 7) surface. *Phys. Rev. Lett.* **76,** 1388–1391 (1996).
19. Palmer, R. E. & Rous, P. J. Resonances in electron scattering by molecules on surfaces. *Rev. Mod. Phys.* **64,** 383–440 (1992).
20. Alavi, S. *et al.* Inducing desorption of organic molecules with a scanning tunneling microscope: theory and experiments. *Phys. Rev. Lett.* **85,** 5372–5375 (2000).
21. Komeda, T., Kim, Y., Fujita, Y., Sainoo, Y. & Kawai, M. Local chemical reaction of benzene on Cu(110) via STM-induced excitation. *J. Chem. Phys.* **120,** 5347–5352 (2004).
22. Jiang, G., Polanyi, J. C. & Rogers, D. Electron and photon irradiation of benzene and chlorobenzene on Si(111)7 × 7. *Surf. Sci.* **544,** 147–161 (2003).
23. Martin, F. *et al.* DNA strand breaks induced by 0–4 eV electrons: the role of shape resonances. *Phys. Rev. Lett.* **93,** 068101 (2004).
24. Dixon-Warren, St-J., Jensen, E. T. & Polanyi, J. C. Direct evidence for charge-transfer photodissociation at a metal surface: CCl_4/Ag(111). *Phys. Rev. Lett.* **67,** 2395–2398 (1991).
25. Palmer, R. E. Electron-molecule dynamics at surfaces. *Prog. Surf. Sci.* **41,** 51–108 (1992).
26. Dressler, R., Allan, M. & Haselbach, E. Symmetry control in bond cleavage processes: dissociative electron attachment to unsaturated halocarbons. *Chimia* **39,** 385–389 (1985).
27. Modelli, A. Electron attachment and intramolecular electron transfer in unsaturated chloroderivatives. *Phys. Chem. Chem. Phys.* **5,** 2923–2930 (2003).
28. Skalicky, T., Chollet, C., Pasquier, N. & Allan, M. Properties of the π^* and σ^* states of the chlorobenzene anion determined by electron impact spectroscopy. *Phys. Chem. Chem. Phys.* **4,** 3583–3590 (2002).
29. Fontanesi, C., Baraldi, P. & Marcaccio, M. On the dissociation dynamics of the benzyl chloride radical anion. An ab initio dynamic reaction coordinate analysis study. *J. Mol. Struct. (Theochem)* **548,** 13–20 (2001).
30. Guyot-Sionnest, P., Dumas, P., Chabal, Y. J. & Higashi, G. S. Lifetime of an adsorbate-substrate vibration: H on Si(111). *Phys. Rev. Lett.* **64,** 2156–2159 (1990).

Acknowledgements We thank the EPSRC and the European Research Training Networks 'Manipulation of individual atoms and molecules' and AMMIST for support. P.A.S. acknowledges studentship support from the School of Physics and Astronomy and from EPSRC. We also thank J. C. Polanyi for pointing us in the direction of vibrationally activated chemical reactions.

Competing interests statement The authors declare that they have no competing financial interests.

Correspondence and requests for materials should be addressed to R.E.P. (r.e.palmer@bham.ac.uk).

Subducted banded iron formations as a source of ultralow-velocity zones at the core–mantle boundary

David P. Dobson & John P. Brodholt

Department of Earth Sciences, University College London, Gower Street, London, WC1E 6BT, UK

Ultralow-velocity zones (ULVZs) are regions of the Earth's core–mantle boundary about 1–10 kilometres thick exhibiting seismic velocities that are lower than radial-Earth reference models by about 10–20 per cent for compressional waves and 10–30 per cent for shear waves. It is also thought that such regions have an increased density of about 0–20 per cent (ref. 1). A number of origins for ULVZs have been proposed, such as ponding of dense silicate melt[2], core–mantle reaction zones[3] or underside sedimentation from the core[4]. Here we suggest that ULVZs might instead be relics of banded iron formations subducted to the core–mantle boundary between 2.8 and 1.8 billion years ago. Consisting mainly of interbedded iron oxides and silica, such banded iron formations were deposited in the world's oceans during the late Archaean and early Proterozoic eras. We argue that these layers, as part of the ocean floor, would be recycled into the Earth's interior by subduction[5], sink to the bottom of the mantle and may explain all of the observed features of ULVZs.

Between 2.8 and 1.8 Gyr ago, the Earth's oceans underwent several periods of oxidation, which are commonly thought to be related to the appearance of photosynthesis in bacteria[6]. Before these oxidation events, ocean waters contained large quantities of (soluble) ferrous iron as a result of chemical weathering of the proto-continents and leaching of the ocean floor near volcanic centres. As primitive life in the form of blue-green algae took hold, oxygen released by photosynthesis would have reacted with the ferrous iron to form magnetite- and haematite-rich sedimentary precipitates: the banded iron formations (BIFs) (Fig. 1). BIFs are the world's most important source of iron, with an estimated 4×10^{14} t globally of 2.5–2.2-billion-year-old BIFs[7]. The most commonly preserved BIFs are interpreted as having been deposited in relatively shallow marine facies, resulting from the interaction between oxidized surface waters and upwelling Fe-rich, reduced deep ocean water, and can be several hundred metres thick. It is likely, however, that a permanent redox front would have existed between oxidized surface waters and reduced iron-rich deep waters in the ocean basins as a whole, not just on continental shelves. Magnetite would precipitate at this front and rain onto the ocean floor forming deep-water BIFs. As part of the ocean floor, these BIFs would then have been recycled into the Earth's interior by subduction[5] (Fig. 2).

The high concentration of iron oxide in BIFs (up to 85 wt%) (ref. 8) results in a density that is greater than any other part of the slab or upper and lower mantle (see below). Subduction processes were certainly occurring at least by the late Archaean, as evidenced by 3.7–2.5-billion-year-old occurrences of boninites and ophiolites[9,10]. Indeed, late Archaean greenstone belts that are interpreted as ophiolites commonly preserve BIFs in the accretionary prism and are interbedded with basaltic magmatism[9,11]. Seismic tomography studies[12] demonstrate that subducted slab material can currently penetrate to the base of the mantle. A similar range of subduction styles are likely to have operated below these ancient subduction zones, transporting at least some BIFs to the core–mantle boundary (CMB).

For subducted BIFs to constitute the ULVZs, a number of physical and chemical criteria must be met. First, BIFs must be negatively buoyant in the mantle. Second, the BIF material must be

able to segregate onto the CMB. Third, BIFs must not react with or dissolve into the core or mantle over the past 3 Gyr. Fourth, the physical properties of BIFs under lower mantle conditions must match those of the ULVZs. And finally, the volume of deep-water BIFs produced and subducted must agree approximately with the volumes of the ULVZs.

The density of a BIF made up of 50% Fe_3O_4 (as magnetite) and 50% SiO_2 (in the quartz, stishovite and columbite phases as appropriate) will be about 3.9 g cm^{-3} on the ocean floor, 5.1 g cm^{-3} at the bottom of the upper mantle (at 2,000 K and 25 GPa) and 6.6 g cm^{-3} in the CMB (at 3,000 K and 136 GPa) (refs 13, 14). Because the oxidation state of the mantle is nearer to iron-wustite than magnetite, it is likely that the Fe_3O_4 component will be reduced to FeO. This would have the effect of increasing the density at the base of the upper mantle to 5.4 g cm^{-3} and to 8.1 g cm^{-3} in the CMB[15,16]. Regardless of the exact phase (NaCl-, NiAs- or inverse (i)NiAs-structured) or oxidation state, the density of the subducting BIF is always much higher than the ambient mantle. At the CMB, the density of a 50% SiO_2, 50% FeO BIF (~8 g cm^{-3}) is higher than the lower mantle (5.6 g cm^{-3}) but less than the outer core (10 g cm^{-3}) (ref. 17), and BIFs are therefore neutrally buoyant between the outer core and lower mantle.

It seems likely, therefore, that BIFs could have been transported into the deep lower mantle by the subduction conveyor belt and that they would tend to sink towards the CMB owing to their high density. In order to be concentrated on the CMB, BIFs would still need to separate from the 100 km or so of silicate slab component. The exact details of this separation are likely to be highly complex. However, one can envisage two simplified end-member processes. In the first, BIF material falls through the underlying slab as diapirs of similar size to the BIF thickness. We can make a conservative estimate that the maximum thickness of BIF deposits preserved on the proto-continents represents the mean depth of BIF deposited in the ocean deeps, about 500 m. A 500 m BIF body will take around 1 Gyr to fall through 100 km of slab with a viscosity of 10^{21} Pa s. This requires that the slab remains at the CMB for about 1 Gyr. The timescales for this would be significantly reduced, however, if the BIF was thickened—owing to, for example, the increased resistance as the slab entered the lower mantle, or mass conserving flow as the slab deforms in response to subduction from a spherical surface. Some models explaining the anomalous Re-Os isotope systematics of ocean island basalts invoke slab material residing at the CMB for billions of years[18], so this timescale for BIF settling may be reasonable. Alternatively, if the slab arrives at the CMB at a steeper angle than about 10° then weak BIF material could separate by flowing along the surface of the slab. If we assume laminar flow of BIF between the slab and overlying mantle, a 500-m-thick layer could settle at 1 cm yr^{-1} if it had a viscosity of 10^{18} Pa s (Supplementary Fig. 1). Once again, increasing the layer thickness enhances the settling rate. This could either cause BIF layers to locally thicken and enhance diapiric settling, or be a direct method for separating the BIFs onto the CMB.

The question then is what would happen to BIFs during subduction and whether they could remain at the CMB for 2 to 3 Gyr. First of all, laser-heated diamond cell measurements[19] show that the FeO melting temperature at 100 GPa is above 5,000 K and FeO will be solid under all mantle conditions. Any reaction with the mantle would, therefore, have to be via a solid-state reaction. The time for a subducting slab to reach the CMB, even if subducting very slowly at 1 cm yr^{-1}, is 300 Myr, sufficient only to diffuse Fe 100 m or so. Even over 3 Gyr, diffusion can only interchange Fe and Mg by about 0.5 km so any sort of solid-state exchange of Fe into the surrounding mantle will not dilute the iron content by any appreciable amount. Assuming BIF arrives at the CMB, will it react or dissolve into the outer core? At the moment the answer to this is not known. If, as has been recently proposed[20], the core formed in oxygen-fugacity equilibrium with the mantle, then the outer core would become more saturated with oxygen with time as the inner core grew, and an FeO component at the CMB could remain stable for the lifetime of the Earth. If, however, the core was undersaturated in oxygen, the FeO component of the BIF would be soluble in the liquid outer core. Even if this were the case, it is not clear that all the FeO would be extracted as dissolution of FeO into the core would leave a residue of (probably) insoluble SiO_2. The FeO-depleted residue could become concentrated at the base of the BIF layer and effectively chemically

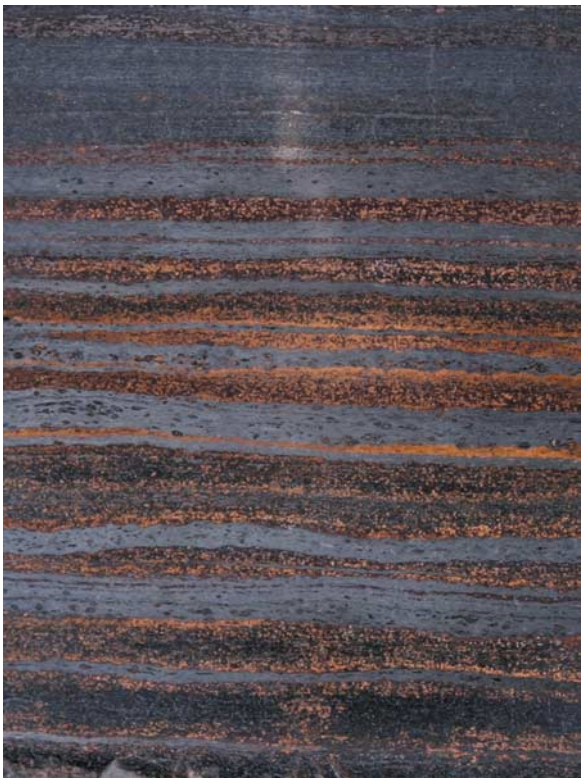

Figure 1 A 2.5-Gyr-old banded iron formation from Hamersley, Australia. The grey bands predominantly contain the iron oxide haematite and the brown bands are rich in siliceous chert.

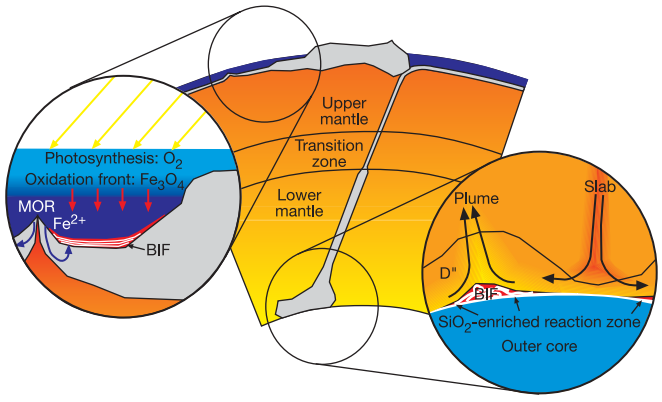

Figure 2 Schematic cross-section of the Earth's mantle showing formation of BIFs in the oceans and segregation at the core–mantle boundary. Left inset, early life in the photic zone of the oceans releases oxygen from the atmosphere by photosynthesis. This reacts with Fe^{2+} in solution in deep ocean waters to produce insoluble iron oxides, which are precipitated as BIF on the ocean floors. BIF is recycled into the mantle at subduction zones. MOR, mid-ocean ridge. Right inset, BIF ponds at the core–mantle boundary, where it is neutrally buoyant. Convection currents concentrate BIF below regions of mantle upwelling where the ultralow-velocity zone is now observed.

isolate the overlying, unreacted BIF. Any reaction zone between the core and mantle is limited to the capillary rise height of the outer core liquid, which is 20 m (ref. 21). Thus a 20-m-thick layer of SiO_2 at the base of any ponded BIF would be sufficient to stop further reaction with the outer core. However, as mentioned above, if the core is saturated or in equilibrium with oxygen, there is no need for such an explanation.

We can now consider whether the physical properties of BIFs are consistent with observations of the ULVZs. The high-pressure/high-temperature seismic properties of the high-pressure FeO phases are not known at present, so we cannot compare directly with the observed reductions in the compressional wave velocity (v_P) and shear wave velocity (v_S). We can, however, estimate the bulk sound velocity (v_ϕ) from the bulk modulus (K) and density (ρ) using the equation ($v_\phi = (K/\rho)^{1/2}$) and compare that to mantle values derived from spherical averaged velocity profiles such as PREM[17]. Pure FeO takes on the NiAs (or iNiAs) structure under CMB conditions[16], but recent experiments[22] suggest that small amounts of MgO can stabilize the low-pressure, NaCl structure. On the basis of the high-pressure equations of state of NiAs- and NaCl-FeO, and stishovite[14–17], we estimate that the bulk sound velocity of BIF will be $9.3 \pm 0.4\,\mathrm{km\,s^{-1}}$, which is 10% slower than PREM values for the base of the mantle. Although the bulk sound velocity is only a rough indicator, not taking into account the shear moduli of the relevant phases, this value is consistent with the seismically observed properties of the ULVZs. Indeed, if BIFs are in the NaCl structure, the recently observed shear-mode softening in FeO (ref. 23) associated with the NaCl–rhombohedral transition will cause a large decrease in v_S relative to v_P, which is one of the most striking properties of the ULVZs.

The final question is whether enough BIFs were produced to account for the observed volume of ULVZs. Again this can only be a rough comparison because first, ULVZs do not appear to be global features in the D″ layer nor has all of D″ been sampled yet, and second, there are no preserved deep-water BIFs (presumably they have been subducted). However, our conservative estimate of deep-ocean BIF thickness, 500 m, would produce a 1.3-km-thick layer if spread evenly along the core–mantle boundary. This is consistent with ULVZ thicknesses of about 5–20 km, over about 12% of the surface of the CMB (ref. 24).

There are still a number of unanswered questions—in particular, can we concentrate thin layers of BIF (~500 m) into layers of a few kilometres thick, consistent with ULVZs, or would it be stretched into even thinner seismically invisible layers? Viscous drag from the base of the mantle would deform weak BIF (or its post-BIF phases) causing it to become concentrated at regions of mantle upwelling, because its gravitational stability at the CMB would inhibit significant entrainment into mantle plumes. In other words, it may pond beneath regions of upwelling, which is consistent with the observation of ULVZs below seismically slow regions of the deep lower mantle[1].

We can now ask the question: what would be the consequences for the dynamics of the CMB if subducted BIF does constitute the ULVZs? FeO is expected to be either a very small-bandgap semiconductor or metallic at mantle pressures and temperatures[18,25], with a large electrical conductivity around 10^4–$10^6\,\mathrm{S\,m^{-1}}$. A 1 km average thickness of subducted BIF would therefore contribute between 10^7 and 10^9 S of conductance to the base of the lower mantle. A laterally varying, highly conductive layer at the base of the mantle, such as that provided by subducted BIF, has been invoked to explain phenomena such as nutations[26] and core–mantle coupling[27]. Small changes in the Earth's length of day that occur on a decadal timescale are attributed to momentum transfer between the core and mantle—core–mantle coupling. One way of achieving this coupling is through interactions of a highly conductive layer at the base of the lower mantle (with 10^8 S of conductance) with the electromagnetic field generated in the core[28]. Normal mantle is insufficiently conductive to be a source of electromagnetic coupling, and silicate or metallic melts have been ruled out[21] as the conductive layer. An ULVZ consisting of the deep BIF assemblage would, however, have the correct properties to explain core–mantle coupling and the other phenomena mentioned above.

The origin of ULVZs remains unknown. We have put forward a hypothesis that may explain all the observed features, although we need further experimental and theoretical data in order to test it. The absence of extensively preserved ocean floor BIFs is explicable in terms of their subduction along with the underlying oceanic crust. We believe that the most likely ultimate fate of subducted BIF is ponding at the core–mantle boundary and that the properties of a deep BIF assemblage can explain observations of ULVZs. One of the most enigmatic features of the deepest interior of the Earth may therefore owe its existence to some of the earliest and most primitive life. □

Received 16 July 2004; accepted 28 January 2005; doi:10.1038/nature03430.

1. Garnero, E. J., Revenaugh, J., Williams, Q., Lay, T. & Kellog, L. H. in *The Core-Mantle Boundary Region* (eds Gurnis, M., Wysession, M. E., Knittle, E. & Buffet, B. A.) 319–334 (American Geophysical Union, Washington DC, 1998).
2. Williams, Q. & Garnero, E. J. Seismic evidence for partial melt at the base of the mantle. *Science* **273,** 1528–1530 (1996).
3. Knittle, E. & Jeanloz, R. Simulating the core-mantle boundary: an experimental study of high-pressure reactions between silicates and liquid iron. *Geophys. Res. Lett.* **16,** 609–612 (1989).
4. Buffett, B. A., Garnero, E. J. & Jeanloz, R. Sediments at the top of Earth's core. *Science* **290,** 1338–1342 (2000).
5. Polat, A., Hofman, A. W. & Rosing, M. T. Boninite-like volcanic rocks in the 3.7–3.8 Ga Isua greenstone belt, West Greenland: geochemical evidence for intra-oceanic subduction zone processes in the early Earth. *Chem. Geol.* **184,** 231–254 (2002).
6. Cloud, P. Paleoecological significance of the banded iron formation. *Econ. Geol.* **68,** 1135–1143 (1973).
7. James, H. L. in *Iron Formation: Facts and Problems* (eds Trendall, A. F. & Morris, R. C.) 472–473 (Elsevier, Amsterdam, 1983).
8. Castro, L. O. Genesis of banded iron-formations. *Econ. Geol.* **89,** 1384–1397 (1994).
9. Kusky, T. M., Li, J.-H. & Tucker, R. D. The Archean Dongandzi Ophiolite Complex, North China Craton: 2.505-billion-year-old oceanic crust and mantle. *Science* **292,** 1142–1146 (2001).
10. Gnaneshwar Rao, T. & Naqvi, S. M. Geochemistry, depositional environment and tectonic setting of the BIF's of the late Archaean Chitradurga Schist Belt, India. *Chem. Geol.* **121,** 217–243 (1995).
11. Taira, A., Pickering, K. T., Windley, B. F. & Soh, W. Accretion of Japanese island arcs and implications for the origin of Archean greenstone belts. *Tectonics* **11,** 1224–1244 (1992).
12. Kárason, H. & Van der Hilst, R. D. in *The History and Dynamics of Global Plate Motion* (eds Richards, M. R., Gordon, R. & Van der Hilst, R. D.) 277–288 (American Geophysical Union, Washington DC, 2000).
13. Mao, H. K., Takahashi, T., Basset, W. A., Kinsland, G. L. & Merrill, L. Isothermal compression of magnetite up to 320 kbar and pressure induced phase transformation. *J. Geophys. Res.* **79,** 1165–1170 (1974).
14. Ross, N. L., Shu, J. F., Hazen, R. M. & Gasparik, T. High-pressure crystal chemistry of stishovite. *Am. Mineral.* **75,** 739–747 (1990).
15. Will, G., Hinze, E. & Nuding, W. The compressibility of FeO measured by energy dispersive X-ray diffraction in a diamond anvil squeezer up to 200 kbar. *Phys. Chem. Miner.* **6,** 157–167 (1980).
16. Fei, Y. W. & Mao, H. K. In-situ determination of the NiAs phase of FeO at high-pressure and temperature. *Science* **266,** 1678–1680 (1994).
17. Dziewonski, A. M. & Anderson, D. L. Preliminary reference Earth model. *Phys. Earth Planet. Inter.* **25,** 297–356 (1981).
18. Hauri, E. H. & Hart, S. R. Re-Os isotope systematics of HIMU and EMII oceanic island basalts from the south-pacific ocean. *Earth Planet. Sci. Lett.* **114,** 353–371 (1993).
19. Knittle, E. & Jeanloz, R. The high pressure phase diagram of $Fe_{0.94}O$: a possible constituent of the Earth's core. *J. Geophys. Res.* **96,** 16169–16180 (1991).
20. Rubie, D. C., Gessmann, C. K. & Frost, D. J. Partitioning of oxygen during core formation on the Earth and Mars. *Nature* **429,** 58–61 (2004).
21. Poirier, J. P., Malavergne, V. & Le Mouël, J. L. in *The Core-Mantle Boundary Region* (eds Gurnis, M., Wysession, M. E., Knittle, E. & Buffet, B. A) 131–138 (American Geophysical Union, Washington DC, 1998).
22. Kondo, T., Ohtani, E., Hirao, N., Yagi, T. & Kikegawa, T. Phase transitions of (Mg,Fe)O at megabar pressures. *Phys. Earth Planet. Inter.* **143–144,** 201–213 (2004).
23. Jacobsen, S. D., Spetzler, H., Reichmann, H. J. & Smyth, J. R. Shear waves in the diamond-anvil cell reveal pressure-induced instability in (Mg,Fe)O. *Proc. Natl Acad. Sci. USA* **101,** 5867–5871 (2004).
24. Persch, S. E. & Vidale, J. E. Reflection properties of the core-mantle boundary from global stacks of *PcP* and *ScP*. *J. Geophys. Res.* **109,** doi:10.1029/2003JB002768 (2004).
25. Knittle, E. & Jeanloz, R. High-pressure metallization of FeO and implications for the Earth's core. *Geophys. Res. Lett.* **13,** 1541–1544 (1986).
26. Buffet, B. A. Constraints on magnetic energy and mantle conductivity from the forced nutations of the Earth. *J. Geophys. Res.* **97,** 19581–19597 (1992).
27. Stix, M. & Roberts, P. H. Time-dependent electromagnetic core-mantle coupling. *Phys. Earth Planet. Inter.* **36,** 49–60 (1984).
28. Holme, R. Electromagnetic core-mantle coupling - I. Explaining decadal changes in the length of day. *Geophys. J. Int.* **132,** 167–180 (1998).

Supplementary Information accompanies the paper on **www.nature.com/nature**.

Acknowledgements We thank P. Bown and M. Kendall for discussions. This work was performed under the auspices of the Deep Earth System Consortium. D.D. was supported by a Royal Society University Research Fellowship.

Competing interests statement The authors declare that they have no competing financial interests.

Correspondence and requests for materials should be addressed to D.P.D. (d.dobson@ucl.ac.uk).

'Lophenteropneust' hypothesis refuted by collection and photos of new deep-sea hemichordates

Nicholas D. Holland[1], David A. Clague[2], Dennis P. Gordon[3], Andrey Gebruk[4], David L. Pawson[5] & Michael Vecchione[6]

[1]*Marine Biology Research Division, Scripps Institution of Oceanography (UCSD), La Jolla, California 92093-0202, USA*
[2]*Monterey Bay Aquarium Research Institute, 7700 Sandholdt Road, Moss Landing, California 95039-9644, USA*
[3]*National Institute of Water and Atmospheric Research, PO Box 14-901, Kilbirnie, Wellington, New Zealand*
[4]*P. P. Shirshov Institute of Oceanology, Russian Academy of Sciences, Nakhimovsky Prospect 36, Moscow 117851, Russia*
[5]*National Museum of Natural History, Smithsonian Institution, Washington, DC 20013-7012, USA*
[6]*NOAA National Systematics Laboratory, National Museum of Natural History, Washington, DC 20013-7012, USA*

The deep ocean is home to a group of broad-collared hemichordates—the so-called 'lophenteropneusts'—that have been photographed gliding on the sea floor[1–8] but have not previously been collected. It has been claimed that these worms have collar tentacles and blend morphological features of the two main hemichordate body plans, namely the tentacle-less enteropneusts and the tentacle-bearing pterobranchs. Consequently, lophenteropneusts have been invoked as missing links to suggest that the former evolved into the latter[5]. The most significant aspect of the lophenteropneust hypothesis is its prediction that the fundamental body plan within a basal phylum of deuterostomes was enteropneust-like. The assumption of such an ancestral state influences ideas about the evolution of the vertebrates from the invertebrates[9–14]. Here we report on the first collected specimen of a broad-collared, deep-sea enteropneust and describe it as a new family, genus and species. The collar, although disproportionately broad, lacks tentacles. In addition, we find no evidence of tentacles in the available deep-sea photographs (published and unpublished) of broad-collared enteropneusts, including those formerly designated as lophenteropneusts. Thus, the lophenteropneust hypothesis was based on misinterpretation of deep-sea photographs of low quality and should no longer be used to support the idea that the enteropneust body plan is basal within the phylum Hemichordata.

The recently collected enteropneust (Figs 1a, b and 2) is described below as a new family, genus and species in the class Enteropneusta of the phylum Hemichordata.

Diagnoses. Torquaratoridae fam. nov.: proboscis and collar each conspicuously broader from side-to-side than in their other dimensions (anteroposterior and dorsoventral); with prominent hepatic caeca, but lacking synapticles.

Torquarator gen. nov.: diagnosis as for family.

Torquarator bullocki n. sp. Description: Living adult 70 mm long and 15 mm wide through collar (smallest length-to-width ratio known for any adult enteropneust). Northeastern Pacific. Colour in life tan anteriorly, grading into light blue posteriorly, except where large white oocytes and dark grey gut contents show through translucent body wall. Proboscis a low dome with breadth (8 mm) conspicuously exceeding anteroposterior or dorsoventral dimensions (both about 5 mm); includes buccal diverticulum (stomochord) and proboscis skeleton with very short anterior and posterior horns; proboscis base encircled by basiepidermal nerve ring. Collar breadth (15 mm) greater than anteroposterior or dorsoventral dimensions (both about 7 mm); wide mouth at anterior end of collar opens into spacious buccal cavity; collar with midventral slit (Fig. 1b, black arrow), paired perihaemal spaces, and collar nerve cord lacking lumen. Trunk accompanied along entire length by lateral wings (sheet-like folds of body wall) and by dorsal and ventral trunk nerves. Lateral wings curling over dorsal surface of trunk in life, but retracting after fixation. Along anterior third of trunk (Fig. 1b, gt), lateral wings include several hundred separate ovaries containing oocytes of diverse sizes; largest oocytes (about 0.5 mm in diameter) white and visible through body wall (Fig. 1a, b). Pharynx (running through anterior 60% of gonadal region) dorsoventrally flattened without subdivision into respiratory region dorsally and digestive region ventrally. Several dozen pharyngeal gill slits in anteroposterior row on either side of dorsal midline with corresponding gill pores in overlying epidermis. No synapticles joining primary and secondary gill bars. Oesophagus (posterior 40% of gonadal region) subdivided into anterior and posterior zones (thin-walled, dorsoventrally flattened) separated by middle zone (thick-walled, circular in cross-section). Intestine, traversing posterior two-thirds of trunk (Fig. 1b, it) as long hepatic region anteriorly (pleated on either side by several dozen hepatic caeca with overlying epidermis closely following their contours) followed by short posterior region (lacking caeca or obvious anal sphincter). In all body regions, musculature poorly developed; epidermal mucus cells uniformly abundant.

Etymology. *Torquarator* derives from the Latin *torques* (collar) plus *arator* (ploughman) and refers to sediment-harvesting by the collar region. The specific name, *bullocki*, honours Professor Theodore Holmes Bullock, who published his PhD dissertation on

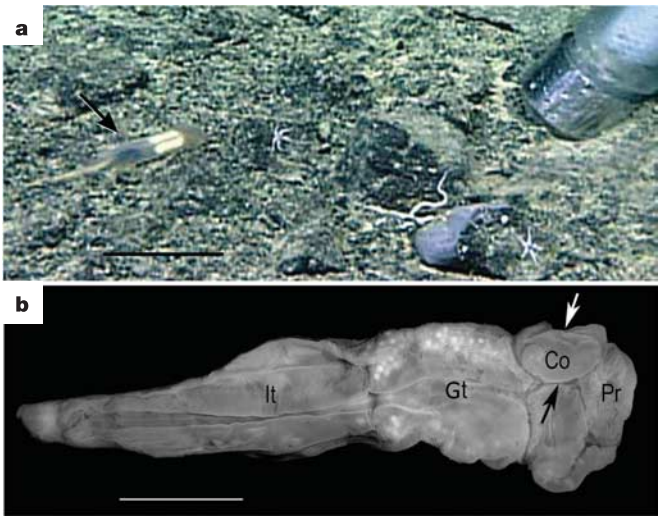

Figure 1 Holotype of *Torquarator bullocki* (Phylum Hemichordata, Class Enteropneusta). **a**, Living specimen (arrowed) crawling on deep-sea floor just before collection by a hose suction sampler (at right). Scale bar, 5 cm. **b**, Ventral view of the same specimen after collection and fixation showing the proboscis (Pr), collar (Co), gonadal trunk region (Gt) and intestinal trunk region (It); the black arrow indicates the midventral slit in the collar, and the white arrow the artefactual compression of the right side of the collar that occurred during capture and fixation. Scale bar, 1 cm.